A Parts Per Billion (ppb) Sensor for NO_2 with Microwatt (μW) Power Requirements based on Micro Light Plates

Olga Casals[1,*], Nicolai Markiewicz[1,2], Cristian Fabrega[1], Isabel Gràcia[4], Carles Cané[4], Hutomo Suryo Wasisto[2,3], Andreas Waag[2,3], Joan Daniel Prades[1]

[1] MIND-IN[2]UB, Department of Electronic and Biomedical Engineering, Universitat de Barcelona, E-08028 Barcelona

[2] IHT-LENA, Technische Universität Braunschweig, D-38106 Braunschweig, Germany

[3] Epitaxy Competence Center (ec[2]), Technische Universität Braunschweig, D-38106 Braunschweig, Germany

[4] IMB-CNM (CSIC), Institut de Microelectrònica de Barcelona, Campus UAB, E-08193 Bellaterra, Spain

ABSTRACT: A film of gas sensitive ZnO nanoparticles has been coupled with a low-power micro light plate (μLP) to achieve a NO_2-parts-per-billion conductimetric gas sensor operating at room temperature. In this μLP configuration, an InGaN-based LED (emitting at 455 nm) is integrated at a few hundred nanometers distance from the sensor material, leading to sensor photoactivation with well controlled, uniform and high irradiance conditions, and very low electrical power needs. The response curves to different NO_2 concentrations as a function of the irradiance displayed a bell-like shape. Responses of 20% to 25 ppb of NO_2 were already observed at irradiances of 5 mWatts·cm^{-2} (applying an electrical power as low as 30 μW). In the optimum illumination conditions (around 60 mWatts · cm^{-2}, or 200 μW of electric power), responses of 94% to 25 ppb were achieved, corresponding to a lower detection limit of 1 ppb of NO_2. Higher irradiance values worsened the sensor response in all the parts-per-billion range of NO_2 concentrations. The responses to other gases such as NH_3, CO and CH_4 were much smaller, showing a certain selectivity towards NO_2. The effects of humidity on the sensor response are also discussed.
KEYWORDS: Gas Sensor, Nitrogen Dioxide (NO_2), High Sensitivity, Photo/Light Activation, Micro Light Plate (μLP), Light Emitting Diode (LED), InGaN, Ultra Low Power.

Nitrogen dioxide (NO_2) is a pollutant gas produced in many of the combustion processes[1] related to heating, industry and transportation, which is object of societal awareness in densely populated areas, especially after public controversies around its emission from diesel engines.

NO_2 is harmful to human health even at concentrations as low as a few hundred parts per billion (ppb)[2], therefore its monitoring requires highly sensitive methods, with very low detection limits. Among the different solutions present in the market, electrochemical and semiconductor sensors are the most widespread. The former ones offer detection limits down to 100 ppb and good specificity (with some cross-sensitivity to O_3 [3]); but are relatively bulky, somehow fragile, and require frequent calibration[4,5]. The latter ones offer similar detectivities in a more robust and much cheaper configuration, but lack of proper specificity and require higher amounts of power to reach the high temperatures needed to come into operation[6,7]. To avoid the need of such heating, it is well-known that some metal oxide (MOX) semiconductor sensors can be operated at room temperature with the help of light activation[8–12]. In fact, it has been demonstrated that light-activated metal oxide sensors can render sensing performances fully equivalent to those obtained with heating[13].

To date, there is a broad literature available reporting light activated MOX sensors for NO_2 [8,9,21–29,13–20]. These works investigate the use of different MOXs (like SnO_2, ZnO, In_2O_3) and MOXs combinations (binary MOX composites, composites of MOXs with catalysts and molecular surface functionalization of MOXs) under different illumination conditions (wavelengths and irradiance levels), and device arrangements (integrated vs. discrete components), being the lowest detection limits reported to date above 100 ppb[13,16]. None of these works addresses the optimization of the power needed to illuminate the sensor material, and either report figures typically above 10 mW or just provide no information about that.

On this regard, we have recently reported on the micro light plate configuration (μLP), which is a sensor architecture built around a miniaturized LED[30]. In the μLP, the sensor material is placed directly on top of a planar LED structure, only separated by a few hundred nanometers to insulate it electrically. Consequently, almost all the light emitted by the LED impinges on the sensor MOX, allowing for very well controlled, uniform and high irradiances, with a reduced electrical power consumption.

In this work, we report on a new NO_2 sensor based on the micro light plate configuration, capable of detecting NO_2 in concentrations ranging from a few parts per billion (ppb) to parts per million (ppm), with power requirements as low as 30 μW. To the best of our knowledge, this is the lowest detection limit reported for light activated metal oxide sensors, and the lowest power consumption as well.

Figure 1.a shows a general view of the μLPs we fabricated. A detailed description about their design and fabrication process can be found elsewhere[30] The μLP exposed four independent pads: two to operate the blue InGaN LED (455 nm peak emission), and two more to measure the electrical resistance of the sensor material lying across a pair of interdigitated electrodes (IDE). As a sensor material, we choose to work with ZnO nanoparticles (maximum size 130 nm, according the specifications provided, Aldrich Prod. No. 721085, CAS Number 1314-13-2)[31,32]. The nanoparticles were deposited on top of the IDEs by micro-drop casting. To that end, we suspended them in diethylene-glycol (CAS Number 111-46-6), which was left to dry in open air at 150°C after the deposition. Following this deposition method, the ZnO nanoparticles displayed a broad light absorption edge in the visible range[31], that overlaps with the LED emission (see Figure 1.e).

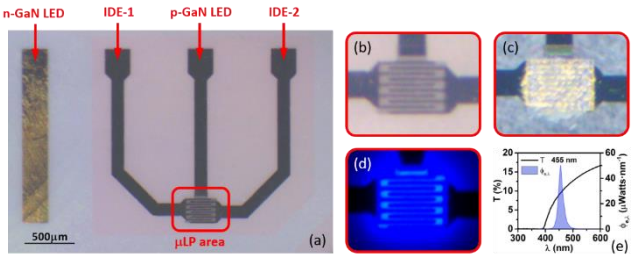

Figure 1. Details of the µLP used in this work. (a) Global view of the device. Metal pads to the p-GaN anode, n-GaN cathode and the IDE pair are shown. The area of the p-GaN mesa can also be seen as a slightly pink-shaded polygon under the IDE-1, p-GaN and IDE-2 pads. The active portion of the µLP device is restricted to the IDE area, containing the sensor material on top, and the LED emitter underneath. See magnified details in (b) bare IDE, (c) ZnO material deposited on top of the IDE , and (d) LED lit on. (e) Light emission spectrum $\phi_{e,\lambda}$ of the InGaN LED in the µLP and light transmission spectrum T of a layer of ZnO NP deposited on a bare sapphire substrate.

To investigate the response to gases of these devices, we introduced them in a gas tight chamber flowing gas blends produced by means of a set of Mass Flow Controllers (MFC, Bronkhorst) at a constant total rate of 400 ml/minute. Reference atmospheres were produced by diluting certified gas patterns in dry synthetic air (SA) (20% O_2 + 80% N_2 in volume ratio, with a purity of 99.999%, H_2O < 5ppm, C_nH_m < 1ppm). Patterns of 10 ppm of NO_2, 100 ppm of NH_3, 100 ppm CO and 1% of CH_4 were used to incorporate the target gases. Relative humidity (RH) –considered at 20ºC and 1 atm– was introduced in some experiments by means of a Controlled Evaporator and Mixer system (CEM, Bronkhorst) by evaporating ultrapure water (> 18 MΩ · cm). The gas chamber was equipped with feedthrough electrical connections to drive the LEDs and to measure the electrical resistance of the MOX layer, by means of a Keithley 2400 sourcemeter SMU. LEDs driving and resistance measurements were carried out under constant current conditions. Ten devices were produced and investigated along several weeks, displaying sensor signal differences of less than 10% before and after the measurement campaign. More details about this experimental set-up can be found elsewhere[33].

Figure 2.a shows a representative resistance record of one of our devices exposed to increasing concentrations of NO_2 ranging from 25 ppb to 1 ppm under steady light irradiance. Clearly, the device is sensitive even to the lowest concentrations available in our setup (25 ppb). A signal to noise ratio analysis suggests that it could be sensitive to concentrations as low as 1 ppb[‡] under the most favorable illumination conditions (i.e. peak sensitivities achieved at 60 mWatts · cm^{-2} with 200 µW of electric power[§]). Figure 2.b summarizes the responses[**] S we obtained to the previous NO_2 concentrations at different optical power levels, expressed in terms of the irradiances E_e impinging on the sensor material. The corresponding values of electric power P_{LED} needed to obtain these irradiance values are shown in the top x-axis (notice that in the case of InGaN-LEDs the relationship between E_e and P_{LED} is not directly proportional[34]). Clearly, the response to gases exhibits a complex bell-shaped dependence with the irradiance/power values, with a maximum signal at E_e values of around 60 mWatts · cm^{-2}, which corresponds to P_{LED} of 200 µW. As discussed in the following lines, this trend is consistent with the models for the photoactivated response of metal oxides to oxidizing gases reported to date, both qualitatively[10], and quantitatively[15].

In the case of NO_2, according to the current literature[10,35], light facilitates charge exchanges with the surface of n-type MOXs following a process like:

$$\left.\begin{aligned} NO_{2(gas)} + e^-_{(ph)} &\rightarrow NO^-_{2(ad)} \\ NO^-_{2(ad)} &\rightarrow NO_{(gas)} + O^-_{(ad)} \\ NO^-_{2(ad)} + e^-_{(ph)} &\rightarrow NO_{(gas)} + O^{2-}_{(ad)} \end{aligned}\right\} \quad (1)$$

where $e^-_{(ph)}$ indicates a free electron in the semiconductor material, generated upon photoexcitation. Real sensing is however carried out in the presence of the oxygen background in air, and O_2 can undergo a similar light-induced process[36]:

$$O_{2(gas)} + e^-_{(ph)} \rightarrow O^-_{2(ad)} \quad (2)$$

Both processes end up trapping negative charges at the MOX surfaces around ionized oxygen adsorbates ($O^-_{(ad)}$, $O^{2-}_{(ad)}$ and $O^-_{2(ad)}$, among others), which can transit trough different molecular and oxidation states until equilibrium is reached, if a supply of free electrons is available (like the ones in the conduction band of an n-type MOX):

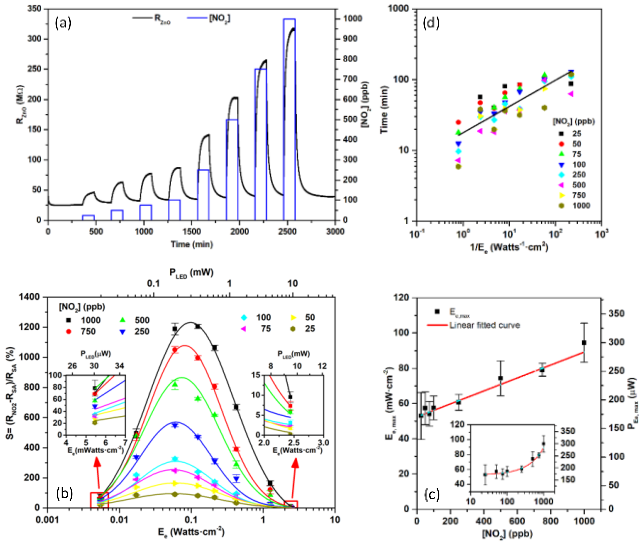

Figure 2. (a) Resistance record of our ZnO NP sensors built on a µLP to increasing concentrations of NO_2, operated at an irradiance E_e of 123 mWatts · cm^{-2}. (b) Summary of the responses S obtained to NO_2 concentrations ranging from 25 ppb to 1 ppm with increasing irradiance/power levels. Bell-shaped solid lines correspond to the fittings to eq.(5). (c) Irradiances $E_{e,MAX}$ at which the maximum response S_{MAX} is reached, as a function of the NO_2 gas concentration. Experimental data follows the linear trend predicted by the models. Experimental data was taken from the fittings in (b), using eq.(6). Error bars were estimated from the statistical fitting uncertainties. Inset shows a semi-log representation of the same dataset. (d) Summary of the response times (defined as the 10% to 90% of the signal rise time) obtained to NO_2 concentrations ranging from 25 ppb to 1 ppm as a function

[‡] To estimate the detection limit, we assumed that signal detection is feasible at values 5 times larger than the noise to signal ratio, which is a common practice in the literature. Since we have a noise level of around 2% (relative to the baseline signal value), we have considered a signal change of at least 10% to extrapolate the lower detection limit.

[§] Optical power units are indicated as Watts (and not as W), in order to easily distinguish them from the electrical power.

[**] We defined the response to gases S as the relative resistance chance in the presence of the target gas, with respect to the value in clean dry SA: $S = \frac{R_{gas} - R_{SA}}{R_{SA}} \cdot 100\ (\%)$

of the invers irradiance ($1/\mathrm{E}_e$). Despite the higher levels of uncertainty, experimental data qualitatively follow the linear trend predicted by eq.(7).

$$\left.\begin{aligned} O^-_{2(ad)} + e^- &\leftrightarrow 2O^-_{(ad)} \\ O^-_{(ad)} + e^- &\leftrightarrow O^{2-}_{(ad)} \end{aligned}\right\} \quad (3)$$

Anyhow, both oxidizing species (NO_2 and O_2) lead to resistance changes in the same direction: increasing the resistance of an n-type MOX by trapping electrons on the surface.

These light-activated detection processes (*adsorption*) compete with a light-activated *desorption* around the oxygen adsorbates resulting from both processes, in the form[36]:

$$O^-_{2(ad)} + h^+_{(ph)} \rightarrow O_{2(gas)} \quad (4)$$

where $h^+_{(ph)}$ indicates a hole in the valence band, generated by an impinging photon.

Therefore, under real operating conditions, the detection of NO_2 is ruled by the competition between (1) NO_2-related oxygen adsorbates, eq.(1), (2) air-related oxygen adsorbates, eq.(2), and (3) their final desorption, eq.(4). Thus, light acts as a moderator of the competition between these reaction paths. These mechanisms have quantitatively predicted the responses S to different concentrations of nitrogen dioxide $[NO_2]$ observed experimentally in n-type MOXs under different light intensities[15].

However, it is only possible to conclude analytic solutions to this model in very simple geometrical configurations (e.g. like one single monocrystalline nanowire). In our case (a thin film of ZnO nanocrystals) the model becomes mathematically untreatable due to the complexity of the electron transport between adjacent randomly-organized crystalline domains. Therefore, we can only expect to fit the dependence of the response S under increasing irradiance E_e levels to a phenomenological bell-shaped trend, that accounts for the counter-balancing of the photoactivated adsorption (that increases with the light intensity, increasing the response) and the photoactivated desorption (that also increases with the light intensity, decreasing the response). Figure 2.b also shows the fitting of our experimental data to a log-normal distribution, in the form:

$$S(\mathrm{E}_e) \propto \frac{1}{\mathrm{E}_e \sigma\sqrt{2\pi}} \cdot exp\{-[ln(\mathrm{E}_e) - \mu]^2/2\sigma^2\} \quad (5)$$

(where μ and σ stand for the mean and standard deviation of $ln(\mathrm{E}_e)$, respectively) observing a good apparent matching ($r > 0.99$ in all cases). Such fitting was purely phenomenological, but allowed us to estimate more accurately the irradiance levels $\mathrm{E}_{e,MAX}$ at which photoadsorption and photodesorption optimally compensate, leading to a maximum in the response S_{MAX}, with

$$\mathrm{E}_{e,MAX} = exp\{\mu - \sigma^2\}\,. \quad (6)$$

Figure 2.c shows that $\mathrm{E}_{e,MAX}$ increases with the gas concentration $[NO_2]$, following a linear trend ($r = 0.992$), as predicted by the models[15]. This is a striking difference compared to conventionally heated sensors, where the temperature that maximizes the response is independent of the gas concentration. This is because, the response of light activated devices involves individual energy packages (the photons) triggering adsorption and desorption events of individual molecules. In contrast, thermal activation has to do with the thermal equilibrium conditions at which the sensor material, as a whole, statistically behaves.

In terms of power consumption, it is remarkable that values as low as 30 μW are enough to observe clear responses to ppb concentrations, with signals well above the noise level. Clearly, slightly higher power values are helpful to develop larger sensor responses (i.e. favoring adsorption processes, eq.(1)), but they still fall in the sub-milliwatt regime (e.g. peak responses S_{MAX} observed between 170 and 300 μW for the gas concentrations investigated). Due to the competitive mechanism discussed before, higher light irradiances lead to lower sensor responses (i.e. excessive desorption, eq.(4)), producing signals below the noise level, and making it pointless to operate the devices at higher power level.

Concerning the dynamic response of the sensors, Figure 2.d summarizes the response times $t_{10\%\rightarrow90\%}$ observed for different gas concentrations $[NO_2]$ and under varying irradiance levels E_e. In this case, the response times decrease monotonously with the light intensity[15], or in other words,

$$t_{10\%\rightarrow90\%} \propto \frac{1}{\mathrm{E}_e}\,. \quad (7)$$

This is because at higher photon arrival rates, the steady balance between photoadsorption and photodesorption of the different molecular species is reached faster. In Figure 2.d, data points were plotted as a function the invers irradiance $1/\mathrm{E}_e$ showing again that experimental data agrees well with pre-existing models for this kind of MOX sensors[15].

It is worth mentioning that our results were obtained with blue light, i.e. with photon energies below the nominal bandgap of ZnO. While this observation is not completely new[21], it is still widely assumed in the literature that electron-hole pair generation by direct bandgap absorption is needed to activate the response to gases of this kind of sensors. The results presented here, however suggest that such assumption might not be necessary, as long as the sensor material offers alternative photogeneration paths (e.g. see Figure 1.e).

We also studied the response of our devices in the presence of humidity, the most common interfering gas in real applications open to atmospheric air. Figure 3.a shows some examples of the resistance records observed upon exposure to NO_2 in different relative humidity (RH) backgrounds. Clearly, the presence of water interferes with the NO_2 sensing mechanism, increasing the response S (Figure 3.b). This is a common and expected effect in MOX sensors of any kind[7], usually attributed to additional reaction paths at the surface enabled by the presence of water-related OH groups. In this case, however, and in contrast to other MOX sensors, humidity leads only to a monotonous rescaling of the sensor signal S, which could be easily removed with the help of an auxiliary humidity sensor. Concerning the response time (Figure 3.b), the presence of water slows it down significantly, even at the lowest RH levels investigated (15%). This deceleration effect does not develop further at higher RH.

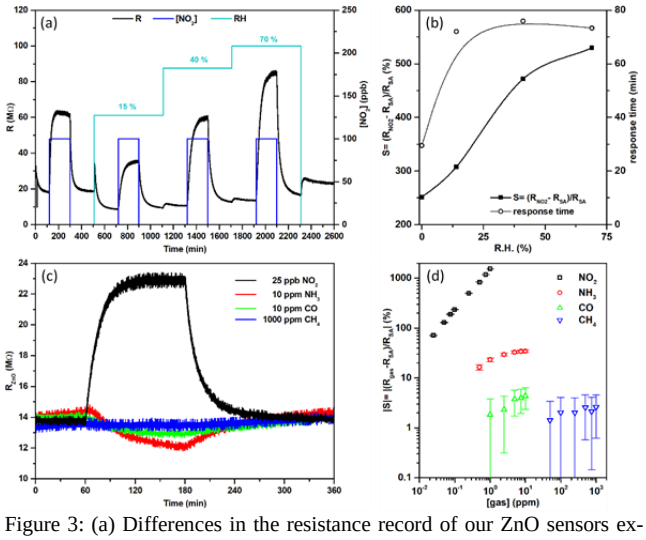

Figure 3: (a) Differences in the resistance record of our ZnO sensors exposed to 100 ppb pulses of NO_2 under increasing relative humidity (RH) backgrounds, and (b) summary of the response magnitudes S and the response times obtained. (c) Exemplary resistance records comparing the responses to NH_3, CO and CH_4, with that to NO_2. Notice that the concentration of NO_2 is much lower than that of the other gases. (d) Full comparison of the responses S obtained to NO_2, NH_3, CO and CH_4 at different concentrations of each gas.

Finally, for completeness, we investigated the response of our sensors to some of the classical gases that are usually monitored with conventional MOX sensors, like NH_3, CO and CH_4. Figure 3.c and Figure 3.d show a comparison between the responses observed to these gases and NO_2. Concentrations were selected to cover the relevant range for each of the gases. Remarkably, our illuminated sensors displayed a much higher response to NO_2 (well over 100% for sub-ppm concentrations) than to all those other gases (below 100% for concentrations well above 1 ppm). These relatively smaller responses, even to higher concentrations of reducing gases, are generally observed in photoactivated gas sensors and may open interesting paths for selectivity improvements[10].

In conclusion, we have presented a gas sensor capable of (1) operating at room temperature, (2) measuring the concentration of NO_2 from a few ppb to ppm (which are record low detection limit and operation range values for this type of sensor), (3) with a power consumption as low 30 μW (again a record value). The sensor was based on the micro light plate (μLP) configuration, which offers a direct path for mass production and industrialization, as it is fully based in microelectronic processing. The material used was ZnO nanoparticles, which are today inexpensive and commercially available. The responses obtained are well described by the models available in the literature and exhibit interfering effects comparable to those of any other MOX-based sensor that could be compensated with additional sources of information (e.g. humidity sensor). Therefore, this development represents a step ahead towards the dream of mass producible, very sensitive, robust and low power gas sensors for NO_2, one of the most socially sound urban pollutants.

AUTHOR INFORMATION

Corresponding Author

Olga Casals, ocasals@el.ub.edu

Notes

The authors declare no competing financial interests.

ACKNOWLEDGMENT

This work has been carried out within the EU Project "BetterSense - Nanodevice Engineering for Better Chemical Gas Sensing Technology" funded by European Research Council under grant agreement no. 336917 and LENA-OptoSense funded by the Lower Saxony Ministry for Science and Culture (N-MWK). O. Casals thanks the support of the TecnioSpring fellowship programme of ACCIÓ, Government of Catalonia, co-funded by the EU Marie Curie Action COFUND. J.D. Prades acknowledges the support of the Serra Húnter Program and the DFG Project GrK NanoMet. This research has made use of the infrastructure of the Spanish ICTS Network MICRONANOFABS partially supported by MINECO.

REFERENCES

(1) Annamalai, K.; Puri, I. K. *Combustion Science and Engineering*; CRC Press: Boca Raton, 2007.

(2) World Health Organization. Nitrogen Dioxide. In *Air Quality Guidelines for Europe-Second Edition*; WHO Regional Office for Europe: Copenhagen, Denmark, 2000; Vol. 3, pp 175–180.

(3) Hossain, M.; Saffell, J.; Baron, R. Differentiating NO_2 and O_3 at Low Cost Air Quality Amperometric Gas Sensors. *ACS Sensors* **2016**, *1* (11), 1291–1294. https://doi.org/10.1021/acssensors.6b00603.

(4) Mead, M. I.; Popoola, O. a M.; Stewart, G. B.; Landshoff, P.; Calleja, M.; Hayes, M.; Baldovi, J. J.; McLeod, M. W.; Hodgson, T. F.; Dicks, J.; et al. The Use of Electrochemical Sensors for Monitoring Urban Air Quality in Low-Cost, High-Density Networks. *Atmos. Environ.* **2013**, *70* (2), 186–203. https://doi.org/10.1016/j.atmosenv.2012.11.060.

(5) Cross, E. S.; Williams, L. R.; Lewis, D. K.; Magoon, G. R.; Onasch, T. B.; Kaminsky, M. L.; Worsnop, D. R.; Jayne, J. T. Use of Electrochemical Sensors for Measurement of Air Pollution: Correcting Interference Response and Validating Measurements. *Atmos. Meas. Tech.* **2017**, *10* (9), 3575–3588. https://doi.org/10.5194/amt-10-3575-2017.

(6) Hsu, L.; Ativanichayaphong, T.; Cao, H.; Sin, J.; Graff, M.; Stephanou, H. E.; Chiao, J. -C. Evaluation of Commercial Metal-oxide Based NO_2 Sensors. *Sens. Rev.* **2007**, *27* (2), 121–131. https://doi.org/10.1108/02602280710731687.

(7) Kumar, R.; Al-Dossary, O.; Kumar, G.; Umar, A. Zinc Oxide Nanostructures for NO2 Gas–sensor Applications: A Review. *Nano-Micro Lett.* **2014**, *7* (2), 1–24. https://doi.org/10.1007/s40820-014-0023-3.

(8) Comini, E.; Cristalli, A.; Faglia, G.; Sberveglieri, G. Light Enhanced Gas Sensing Properties of Indium Oxide and Tin Dioxide Sensors. *Sensors Actuators, B Chem.* **2000**, *65* (1), 260–263. https://doi.org/10.1016/S0925-4005(99)00350-0.

(9) Comini, E.; Faglia, G.; Sberveglieri, G. UV Light Activation of Tin Oxide Thin Films for NO2 Sensing at Low Temperatures. *Sensors Actuators, B Chem.* **2001**, *78* (1–3), 73–77. https://doi.org/10.1016/S0925-4005(01)00796-1.

(10) Espid, E.; Taghipour, F. UV-LED Photo-Activated Chemical Gas Sensors: A Review. *Crit. Rev. Solid State Mater. Sci.* **2017**, *42* (5), 416–432. https://doi.org/10.1080/10408436.2016.1226161.

(11) Kumar, R.; Goel, N.; Kumar, M. UV-Activated MoS2 Based Fast and Reversible NO2 Sensor at Room Temperature. *ACS Sensors* **2017**, *2* (11), 1744–1752. https://doi.org/10.1021/acssensors.7b00731.

(12) Kumar, M. M.; Agrawal, A. V.; Kumar, R.; Venkatesan, S.; Zakhidov, A.; Yang, G.; Bao, J.; Kumar, M. M. Photoactivated Mixed In-Plane and Edge-Enriched p-Type MoS2 Flake-Based NO2 Sensor Working at Room Temperature. *ACS Sensors* **2018**, *3* (5), 998–1004. https://doi.org/10.1021/acssensors.8b00146.

(13) Prades, J. D.; Jimenez-Diaz, R.; Hernandez-Ramirez, F.; Barth, S.; Cirera, a.; Romano-Rodriguez, a.; Mathur, S.; Morante, J. R. Equivalence between Thermal and Room Temperature UV Light-Modulated Responses of Gas Sensors Based on Individual SnO2 Nanowires. *Sensors Actuators B Chem.* **2009**, *140* (2), 337–341. https://doi.org/10.1016/j.snb.2009.04.070.

(14) Anothainart, K.; Burgmair, M.; Karthigeyan, A.; Zimmer, M.; Eisele, I. Light Enhanced NO2 Gas Sensing with Tin Oxide at Room Temperature: Conductance and Work Function Measurements. *Sensors Actuators B Chem.* **2003**, *93* (1–3), 580–584. https://doi.org/10.1016/S0925-4005(03)00220-X.

(15) Prades, J. D.; Jimenez-Diaz, R.; Manzanares, M.; Hernandez-Ramirez, F.; Cirera, A.; Romano-Rodriguez, A.; Mathur, S.; Morante, J. R. A Model for the Response towards Oxidizing Gases of Photoactivated Sensors Based on Individual SnO2 Nanowires. *Phys. Chem. Chem. Phys.* **2009**, *11* (46), 10881–10889. https://doi.org/10.1039/b915646a.

(16) Lu, G.; Xu, J.; Sun, J.; Yu, Y.; Zhang, Y.; Liu, F. UV-Enhanced Room Temperature NO2 Sensor Using ZnO Nanorods Modified with SnO2 Nanoparticles. *Sensors Actuators, B Chem.* **2012**, *162* (1), 82–88. https://doi.org/10.1016/j.snb.2011.12.039.

(17) Wagner, T.; Kohl, C. D.; Morandi, S.; Malagú, C.; Donato, N.; Latino, M.; Neri, G.; Tiemann, M. Photoreduction of Mesoporous In2O3: Mechanistic Model and Utility in Gas Sensing. *Chem. - A Eur. J.* **2012**, *18* (26), 8216–8223. https://doi.org/10.1002/chem.201103905.

(18) Wagner, T.; Kohl, C. D.; Malagù, C.; Donato, N.; Latino, M.; Neri, G.; Tiemann, M. UV Light-Enhanced NO2 Sensing by Mesoporous In2O3: Interpretation of Results by a New Sensing Model. *Sensors Actuators, B Chem.* **2013**, *187* (2), 488–494. https://doi.org/10.1016/j.snb.2013.02.025.

(19) Park, S.; An, S.; Mun, Y.; Lee, C. UV-Enhanced NO2 Gas Sensing Properties of SnO2-Core/ZnO-Shell Nanowires at Room Temperature. *ACS Appl. Mater. Interfaces* **2013**, *5* (10), 4285–4292. https://doi.org/10.1021/am400500a.

(20) Mun, Y.; Park, S.; An, S.; Lee, C.; Kim, H. W. NO2 Gas Sensing Properties of Au-Functionalized Porous ZnO Nanosheets Enhanced by UV Irradiation. *Ceram. Int.* **2013**, *39* (8), 8615–8622. https://doi.org/10.1016/j.ceramint.2013.04.035.

(21) Zhang, C.; Boudiba, A.; De Marco, P.; Snyders, R.; Olivier, M. G.; Debliquy, M. Room Temperature Responses of Visible-Light

Illuminated WO3 Sensors to NO2 in Sub-Ppm Range. *Sensors Actuators, B Chem.* **2013**, *181*, 395–401. https://doi.org/10.1016/j.snb.2013.01.082.

(22) Park, S.; Ko, H.; Lee, S.; Kim, H.; Lee, C. Light-Activated Gas Sensing of Bi2O3-Core/ZnO-Shell Nanobelt Gas Sensors. *Thin Solid Films* **2014**, *570* (PB), 298–302. https://doi.org/10.1016/j.tsf.2014.02.110.

(23) Hoffmann, M. W. G.; Prades, J. D.; Mayrhofer, L.; Hernandez-Ramirez, F.; Järvi, T. T.; Moseler, M.; Waag, A.; Shen, H. Highly Selective SAM-Nanowire Hybrid NO2 Sensor: Insight into Charge Transfer Dynamics and Alignment of Frontier Molecular Orbitals. *Adv. Funct. Mater.* **2014**, *24* (5), 595–602. https://doi.org/10.1002/adfm.201301478.

(24) Hoffmann, M. W. G.; Mayrhofer, L.; Casals, O.; Caccamo, L.; Hernandez-Ramirez, F.; Lilienkamp, G.; Daum, W.; Moseler, M.; Waag, A.; Shen, H.; et al. A Highly Selective and Self-Powered Gas Sensor Via Organic Surface Functionalization of p-Si/n-ZnO Diodes. *Adv. Mater.* **2014**, *26* (47), 8017–8022. https://doi.org/10.1002/adma.201403073.

(25) Fabbri, B.; Gaiardo, A.; Giberti, A.; Guidi, V.; Malagù, C.; Martucci, A.; Sturaro, M.; Zonta, G.; Gherardi, S.; Bernardoni, P. Chemoresistive Properties of Photo-Activated Thin and Thick ZnO Films. *Sensors Actuators, B Chem.* **2014**, *222*, 1251–1256. https://doi.org/10.1016/j.snb.2015.06.048.

(26) Saboor, F. H.; Ueda, T.; Kamada, K.; Hyodo, T.; Mortazavi, Y.; Khodadadi, A. A.; Shimizu, Y. Enhanced NO2 Gas Sensing Performance of Bare and Pd-Loaded SnO2 Thick Film Sensors under UV-Light Irradiation at Room Temperature. *Sensors Actuators, B Chem.* **2016**, *223* (2), 429–439. https://doi.org/10.1016/j.snb.2015.09.075.

(27) Hyodo, T.; Urata, K.; Kamada, K.; Ueda, T.; Shimizu, Y. Semiconductor-Type SnO2-Based NO2 Sensors Operated at Room Temperature under UV-Light Irradiation. *Sensors Actuators, B Chem.* **2017**, *253* (2), 630–640. https://doi.org/10.1016/j.snb.2017.06.155.

(28) Espid, E.; Taghipour, F. Development of Highly Sensitive ZnO/In2O3 Composite Gas Sensor Activated by UV-LED. *Sensors Actuators, B Chem.* **2017**, *241*, 828–839. https://doi.org/10.1016/j.snb.2016.10.129.

(29) Espid, E.; Taghipour, F. Facile Synthesis and UV-Activated Gas Sensing Performance of Ag:ZnO Nano-Ellipsoids. *ECS J. Solid State Sci. Technol.* **2018**, *7* (7), Q3089–Q3093. https://doi.org/10.1149/2.0141807jss.

(30) Markiewicz, N.; Casals, O.; Fabrega, C.; Gràcia, I.; Cané, C.; Suryo, H.; Waag, A.; Prades, J. D. Micro Light Plates for Low-Power Photoactivated Gas Sensors. *Appl. Phys. Lett.* **2019**, *114*, 053508. https://doi.org/10.1063/1.5078497.

(31) Zhang, Q.; Park, K.; Cao, G. Synthesis of ZnO Aggregates and Their Application in Dye-Sensitized Solar Cells. *Mater. Matters* **2010**, *5* (2), 32–40.

(32) Rossi, T.; Penfold, T. J.; Rittmann-Frank, M. H.; Reinhard, M.; Rittmann, J.; Borca, C. N.; Grolimund, D.; Milne, C. J.; Chergui, M. Characterizing the Structure and Defect Concentration of ZnO Nanoparticles in a Colloidal Solution. *J. Phys. Chem. C* **2014**, *118* (33), 19422–19430. https://doi.org/10.1021/jp505559u.

(33) Casals, O.; Becker, T.; Godignon, P.; Romano-Rodriguez, A. SiC-Based MIS Gas Sensor for High Water Vapor Environments. *Sensors Actuators, B Chem.* **2012**, *175*, 60–66. https://doi.org/10.1016/j.snb.2011.12.032.

(34) Karpov, S. ABC-Model for Interpretation of Internal Quantum Efficiency and Its Droop in III-Nitride LEDs: A Review. *Opt. Quantum Electron.* **2015**, *47* (6), 1293–1303. https://doi.org/10.1007/s11082-014-0042-9.

(35) Karaduman, I.; Yildiz, D. E.; Sincar, M. M.; Acar, S. UV Light Activated Gas Sensor for NO2 Detection. *Mater. Sci. Semicond. Process.* **2014**, *28* (2), 43–47. https://doi.org/10.1016/j.mssp.2014.04.011.

(36) Fan, S. W.; Srivastava, A. K.; Dravid, V. P. UV-Activated Room-Temperature Gas Sensing Mechanism of Polycrystalline ZnO. *Appl. Phys. Lett.* **2009**, *95* (14), 1–4. https://doi.org/10.1063/1.3243458.

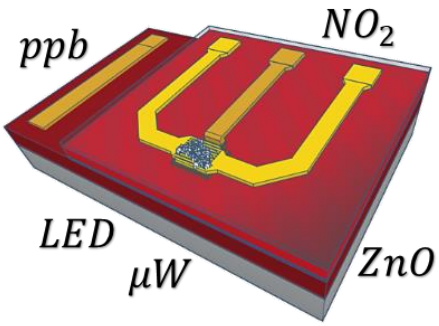

for TOC only